

A Record of Large Earthquakes on the Southern Hayward Fault for the Past 500 Years

by James J. Lienkaemper, Timothy E. Dawson, Stephen F. Personius, Gordon G. Seitz,
Liam M. Reidy, and David P. Schwartz

Abstract The Hayward fault, a major branch of the right-lateral San Andreas fault system, traverses the densely populated eastern San Francisco Bay region, California. We conducted a paleoseismic investigation to better understand the Hayward fault's past earthquake behavior. The site is near the south end of Tyson's Lagoon, a sag pond formed in a right step of the fault in Fremont. Because the Hayward fault creeps at the surface, we identified paleoseismic events using features that we judge to be unique to ground ruptures or the result of strong ground motion, such as the presence of fault-scarp colluvial deposits and liquefaction. We correlate the most recent event evidence (E1) to the historical 1868 **M** 6.9 earthquake that caused liquefaction in the pond and recognize three additional paleoruptures since A.D. 1470 \pm 110 yr. Event ages were estimated by chronological modeling, which incorporated historical and stratigraphic information and radiocarbon and pollen data. Modeled, mean age and 95-percentile ranges of the three earlier events are A.D. 1730 (1650–1790) yr (E2), A.D. 1630 (1530–1740) yr (E3), and A.D. 1470 (1360–1580) (E4). The ages of these paleoearthquakes yield a mean recurrence of 130 \pm 40 yr. Although the mean recurrence is well determined for the period A.D. 1470–1868, individual intervals are less well determined: E1–E2, 140 + 80/–70 yr; E2–E3, 100 + 90/–100 yr; and E3–E4, 150 + 130/–110 yr.

Introduction

We present evidence for recurrence intervals of large earthquakes on the southern Hayward fault at Tyson's Lagoon, also called Tule Pond, a large (0.8 km \times 0.15 km) sag pond formed in a right step in the fault (Figs. 1, 2). Determination of earthquake recurrence from geologic evidence of past large earthquakes is essential for improving understanding of fault behavior and regional earthquake cycles, particularly in the San Francisco Bay area with its short, 225-yr historical seismic record. Earthquake recurrence is also critical input to estimates of earthquake probability (e.g., the Working Group on California Earthquake Probabilities, 1999 [WG99]) and seismic hazards mapping (Frankel *et al.*, 2000). The Hayward fault (Fig. 1) is a major branch of the San Andreas fault system and traverses the densely populated eastern San Francisco Bay region. For at least several decades the Hayward fault has been creeping at the surface at an average rate of 4.6 \pm 0.5 mm/yr (averaged along the fault over several decades) (Lienkaemper *et al.*, 2001). The average creep rate is about half its long-term slip rate of 9 \pm 2 mm/yr (Lienkaemper and Borchardt, 1996; WG99). The fault is composed of two sections. The southern Hayward fault produced a major surface-rupturing earthquake in 1868 (**M** 6.8: Bakun [1999]; **M** 7.0: Yu and Segall

[1996]; herein averaged as **M** 6.9). The 1868 earthquake had a geodetically estimated, mean dextral slip of 1.9 \pm 0.4 m, (Yu and Segall, 1996) and an estimated rupture length of 45–60 km (Fig. 1) (Lienkaemper and Galehouse, 1998). Although the northern Hayward fault has produced no major historical earthquakes, it has produced several large ruptures in the past 2000 yr (Hayward Fault Paleoseismic Group, 1999).

Tyson's Lagoon has been the location of deposition throughout much of the Holocene and the stratigraphic record preserved in it provides an excellent environment for investigating paleoearthquakes. At present, it is the last remaining unurbanized location on the southern part of the fault where paleoseismic data can be obtained. Several previous trenching investigations have been conducted here (Fig. 2). Early trenching at the south end of the pond by Woodward-Clyde and Associates (1970) (Fig. 3) for fault hazard zoning indicated that the southwestern fault trace had produced substantially greater deformation in sediment younger than 1000 yr than the northeastern trace. At the north end of the Tule Pond, Williams (1993) studied the northeastern fault trace and produced the first paleoseismic observations for the occurrence of individual late Holocene

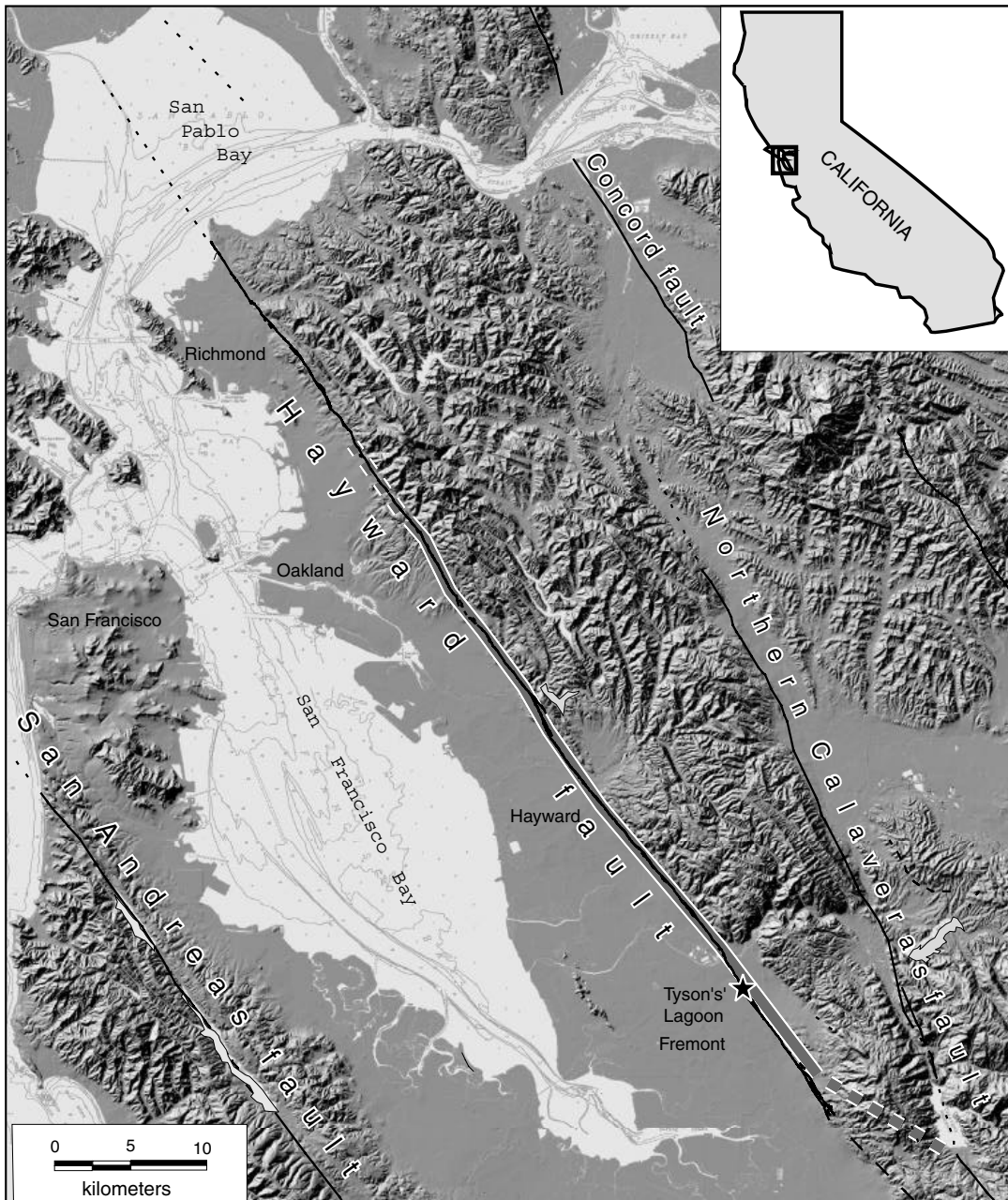


Figure 1. Site location map. Gray band along Hayward fault from Oakland to Fremont indicates approximate extent of 1868 rupture (Lienkaemper and Galehouse, 1998).

earthquakes. Using brittle deformation and liquefaction features, he interpreted the occurrence of six to eight large earthquakes during the past approximately 2.1 ka, with three events (including the 1868 earthquake) during the past 500 years. Because of limited high-resolution stratigraphy, as well as large chronological uncertainties, the ages of individual events were less well constrained than in this study. Reconnaissance trenching by J. N. Alt (unpublished data, 1998) indicated unusually rapid sedimentation along the southwestern trace on the south end of the pond (Fig. 3). Rapid deposition relative to the rate of deformation can pro-

duce stratigraphy with the potential to distinguish creep from brittle, coseismic deformation, so we chose to perform a detailed study at the same location.

Our ongoing investigation has thus far focused on the identification and dating of paleoearthquakes during the past 500 yr, a time period for which we have constraining ages on buried ground surfaces that were disrupted by faulting. The entire data set, consisting of detailed trench logs, descriptions of methodology, and radiocarbon and pollen data is too large to present here and is available at <http://geopubs.wr.usgs.gov/map-mf/mf2386/> (Lienkaemper *et al.*

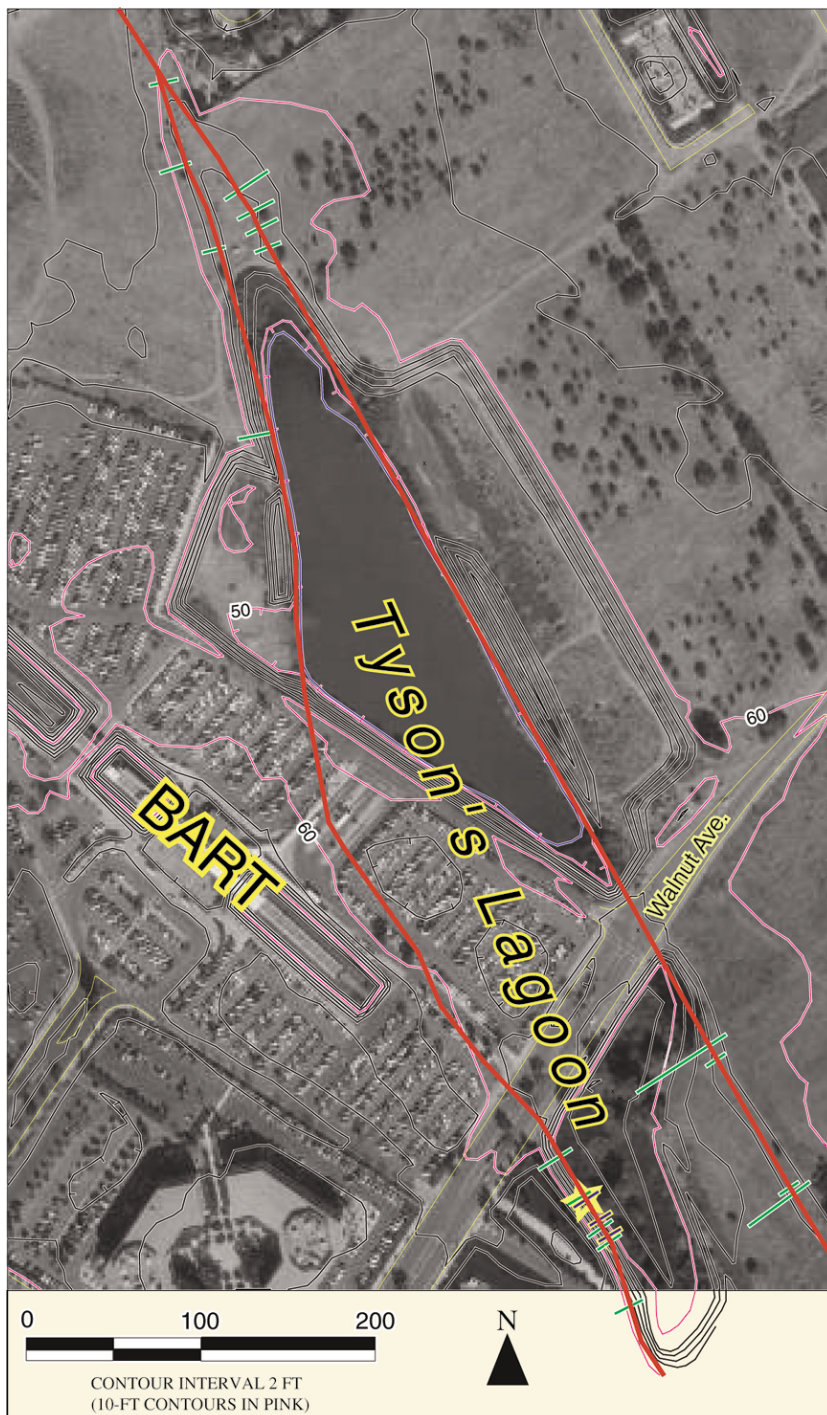


Figure 2. Map showing the Hayward fault (red), which forms a closed depression or sag pond called Tyson's Lagoon (Tule Pond). Earlier trenches shown in green (Lienkaemper, 1992). Star indicates location of trench 00A. See Figure 3 for detail of trench locations.

2002). In this article we first discuss the setting of the site and the observations used to identify earthquake event horizons and distinguish coseismic rupture from fault creep. Then we describe the chronological model approach used to constrain the timing of the identified events and earthquake recurrence intervals. Lastly, we discuss the possible sizes of these past earthquakes and implications of our observations for the behavior of the southern Hayward fault.

Trench Site Setting

Despite urban modification of much of Tyson's Lagoon, our trenching investigation revealed excellent exposures of deformed late Holocene sediments on the Hayward fault. At our site south of Walnut Avenue, the southwestern trace is marked by a linear, 2- to 3-m-high east-facing fault scarp. We excavated three trenches across the base of this scarp (Fig. 3), exposing a complex near-vertical shear zone developed in late Quaternary(?) sandy alluvial sediments



Figure 3. Map showing trench locations along the Hayward fault at Tyson's Lagoon, south of Walnut Avenue in Fremont, California. Labels: 70A–70G, Woodward-Clyde and Associates (1970); 98A–98B, J. N. Alt (unpublished, 1998); 00A–00C, this study.

(Lienkaemper *et al.*, 2002). A strong oblique component of deformation is expressed as a several-meter-wide zone of shallow apparent thrust faults rooted in the main fault zone that upwarps adjacent pond sediments just east of the main shear zone (Figs. 4–7). A graben filled with late Holocene sediment is formed between the main trace and an antithetic normal-oblique fault zone a few meters to the east. This graben is as much as five meters wide in trench 00A (Figs. 4, 5), but narrows to less than 1 m in trench 00C (logs of trenches 00B and 00C in Lienkaemper *et al.* [2002]). The sediment-filled graben and the antithetic fault zone that forms its eastern margin show no surface expression on the floor of Tyson's Lagoon. Fortunately, the graben is filled with more than 2 m of late Holocene sediment that contains an excellent preserved record of deformation along this strand of the southern Hayward fault.

Tyson's Lagoon is formed in fluvial silt, sand, and gravel deposits associated with the Niles alluvial cone, a broad, latest Quaternary(?) fan that emanates from the mouth of nearby Niles Canyon (California Department of Water Resources, 1967). These relatively coarse sediments are exposed in the fault scarps that bound the margins of the pond.

The pond sediments exposed in our trenches primarily consist of well-bedded deposits of silty clay, interbedded with organic and shell rich layers, and slightly coarser, less organic silts and sandy silts. The fine grain texture and well-preserved bedding suggest that these deposits were mostly locally derived sediment deposited in a subsiding, shallow water environment that currently is subject to seasonal desiccation. These deposits thicken across the rapidly deforming graben adjacent to the main fault zone and show distinct variations in color, grain size, and organic content. Sedimentologic evidence of deformation associated with surface rupture and strong ground shaking in the graben deposits includes soft-sediment deformation or liquefaction of silts and sandy silts and formation of several blocky scarp colluvial units adjacent to the main fault zone. These stratigraphic features form the basis for our paleoseismic interpretations. A more detailed description of the depositional sequence is contained in Appendix 1.

Evidence for Paleoearthquakes

The Hayward fault creeps at the surface at about half its long-term slip rate. Presumably, the deficit between the long-term slip rate and aseismic creep is released in large surface-rupturing earthquakes such as the 1868 earthquake. Thus, the Hayward fault presents a challenge in paleoseismology because we need to distinguish evidence of distinct coseismic surface ruptures associated with paleoearthquakes from deformation produced by interseismic creep. Previous studies along creeping faults have attempted to distinguish between features generated by creep and features created by coseismic rupture with equivocal results (Hay *et al.*, 1989; Stenner and Ueta, 2000). Several types of evidence that may be indicative of the occurrence of a ground-rupturing event along a fault accompanying a large earthquake may become moot for creeping fault traces (Kelson and Baldwin, 2001). Commonly used indicators of “event” horizons include liquefaction, upward terminations of faulting, and abrupt changes in deformation between units. Each of these types of evidence, taken alone, might otherwise be explained by off-fault seismic sources or fault creep. Liquefaction can occur as a result of strong shaking produced by earthquakes on other faults. If creep accumulates over several decades both as slip and folding without deposition, subsequent burial of the deformed surface could yield both upward terminations and undeformed strata overlying strata that has been deformed. Consequently, along a fault that exhibits creep, these forms of event evidence do not necessarily prove the occurrence of surface-rupturing earthquakes.

Lines of paleoseismic evidence that may be unique to coseismic rupture and not creep include fissure fills and colluvial-wedge deposits (Stenner and Ueta, 2000; Kelson and Baldwin, 2001). In Italy, Ferrelle *et al.* (2002) used several lines of stratigraphic evidence to differentiate between coseismic and aseismic slip. Trench exposures along the rapidly creeping (2 cm/yr) Pernicana fault lacked any evidence

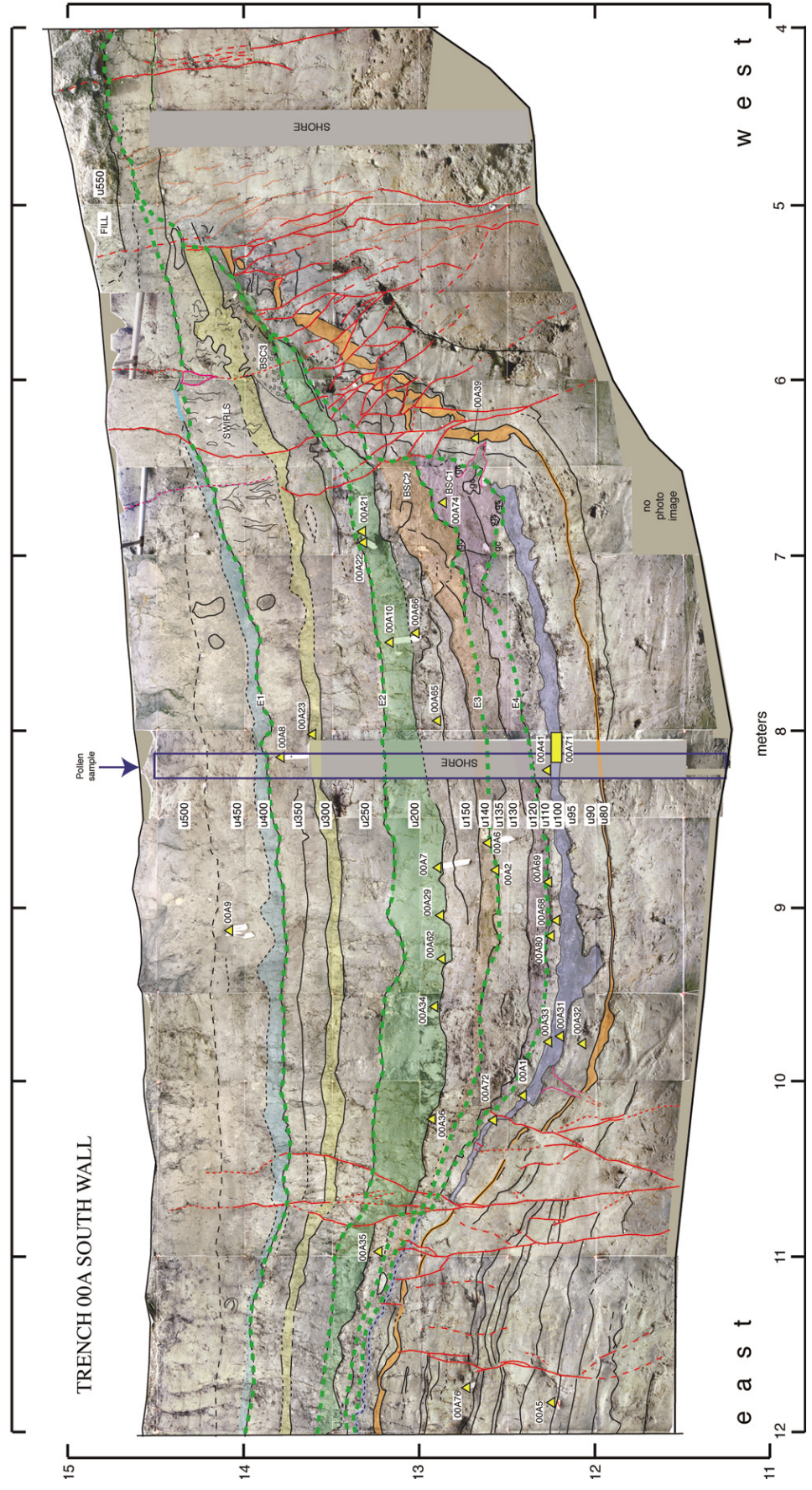


Figure 4. Log of a portion of the south wall of trench 00A showing: faults in red; event horizons (E1, E2, E3, E4) as dashed green lines; carbon samples as yellow triangles, rectangle for bulk samples. Tinted key marker units, labeled u80, u100, u200, u300, and u400, are composed of organic silty clay. Distinct blocky scarp colluvia labelled BSC1, BSC2, and BSC3 were produced following events E4, E3, and E2; E1 horizon (base of u400) was the ground surface at the time of the 1868 earthquake. Continuous pollen sample location outlined in blue at station 8 m. Other abbreviations: cl, clay; gv, gray clay; gc, gray clay; rk, rock; sd, sand; st, silt.

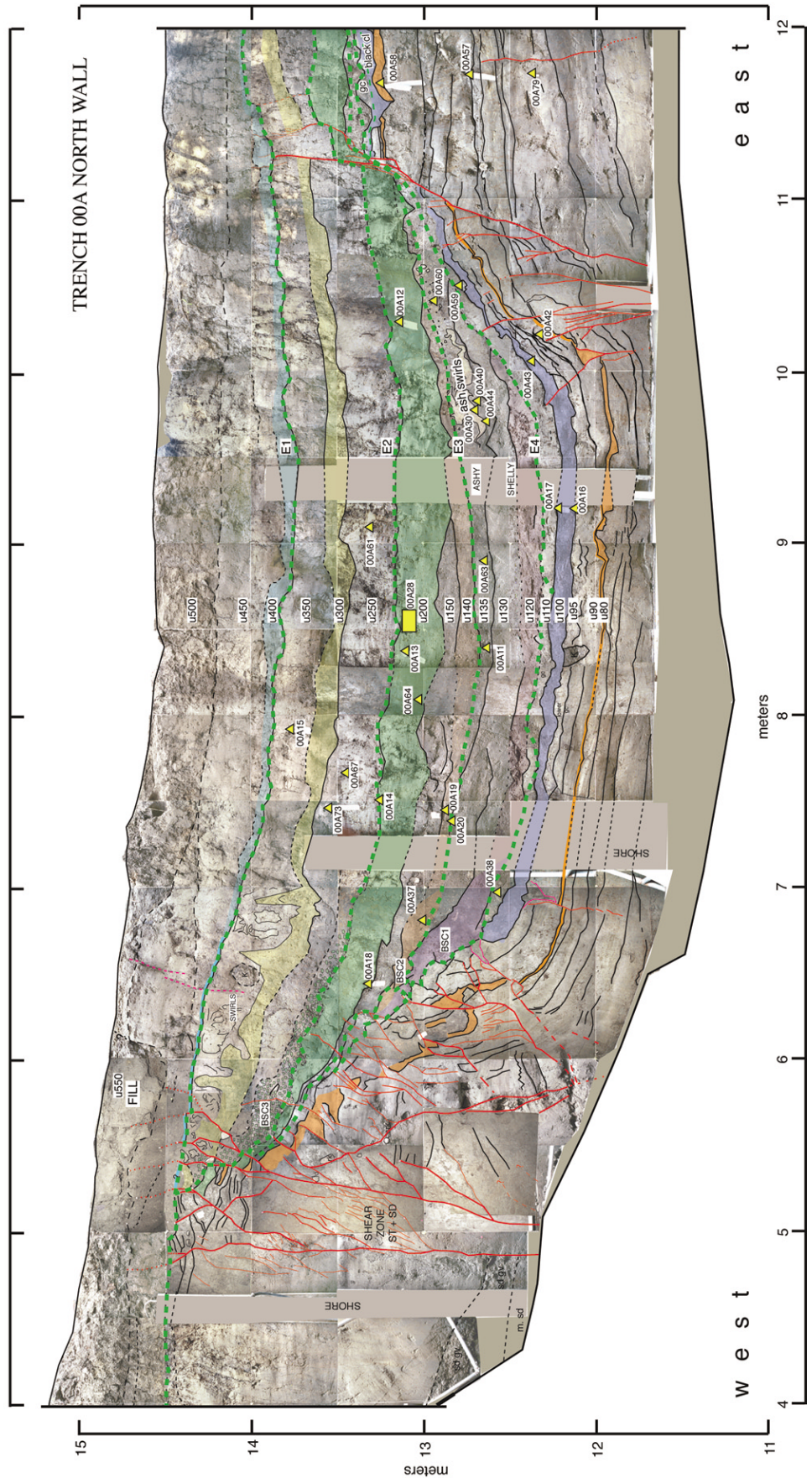


Figure 5. Log of north wall of Trench 00A. Has same scale and other features as in Figure 2.

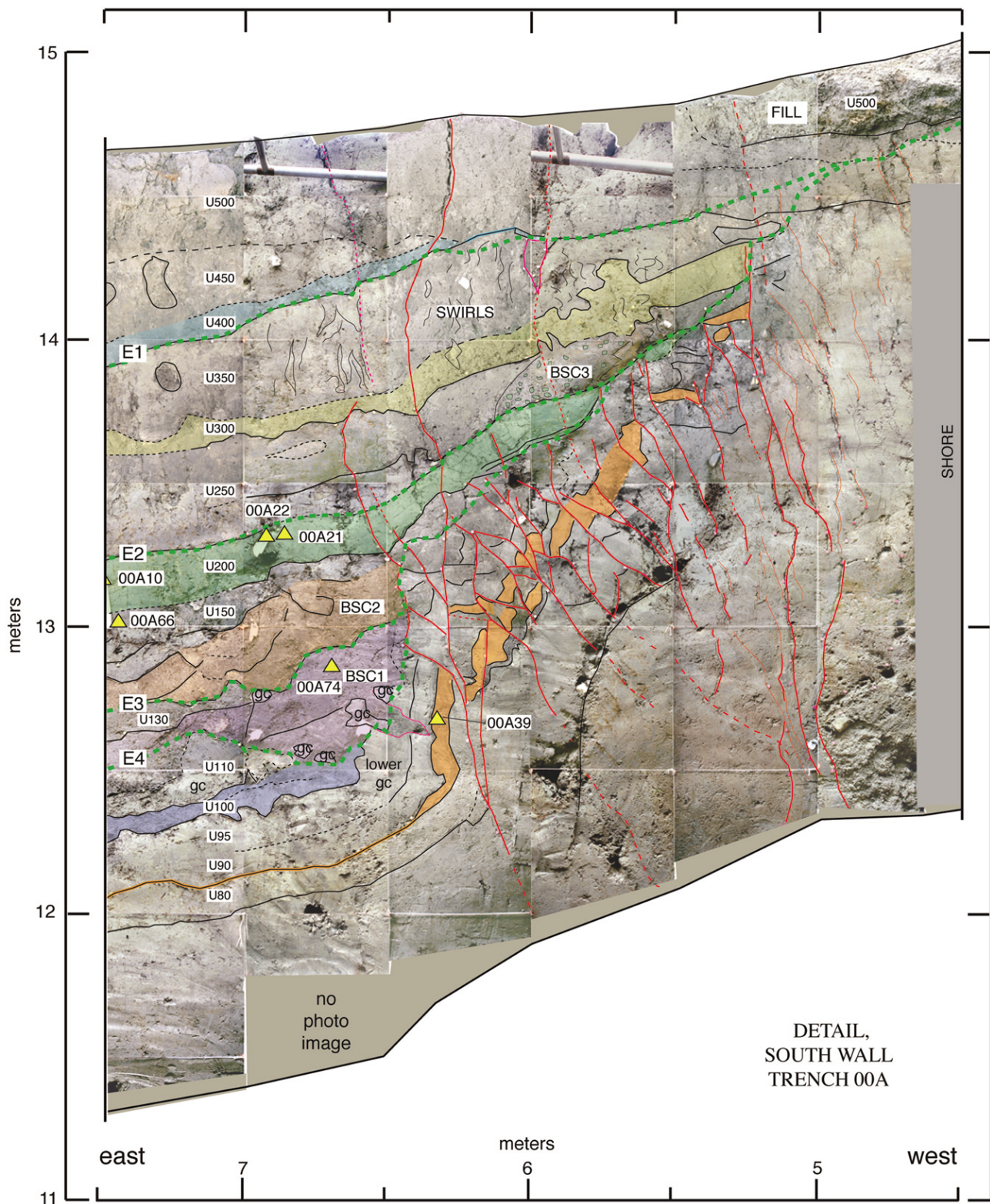


Figure 6. Enlargement of main fault trace on the south wall of trench 00A.

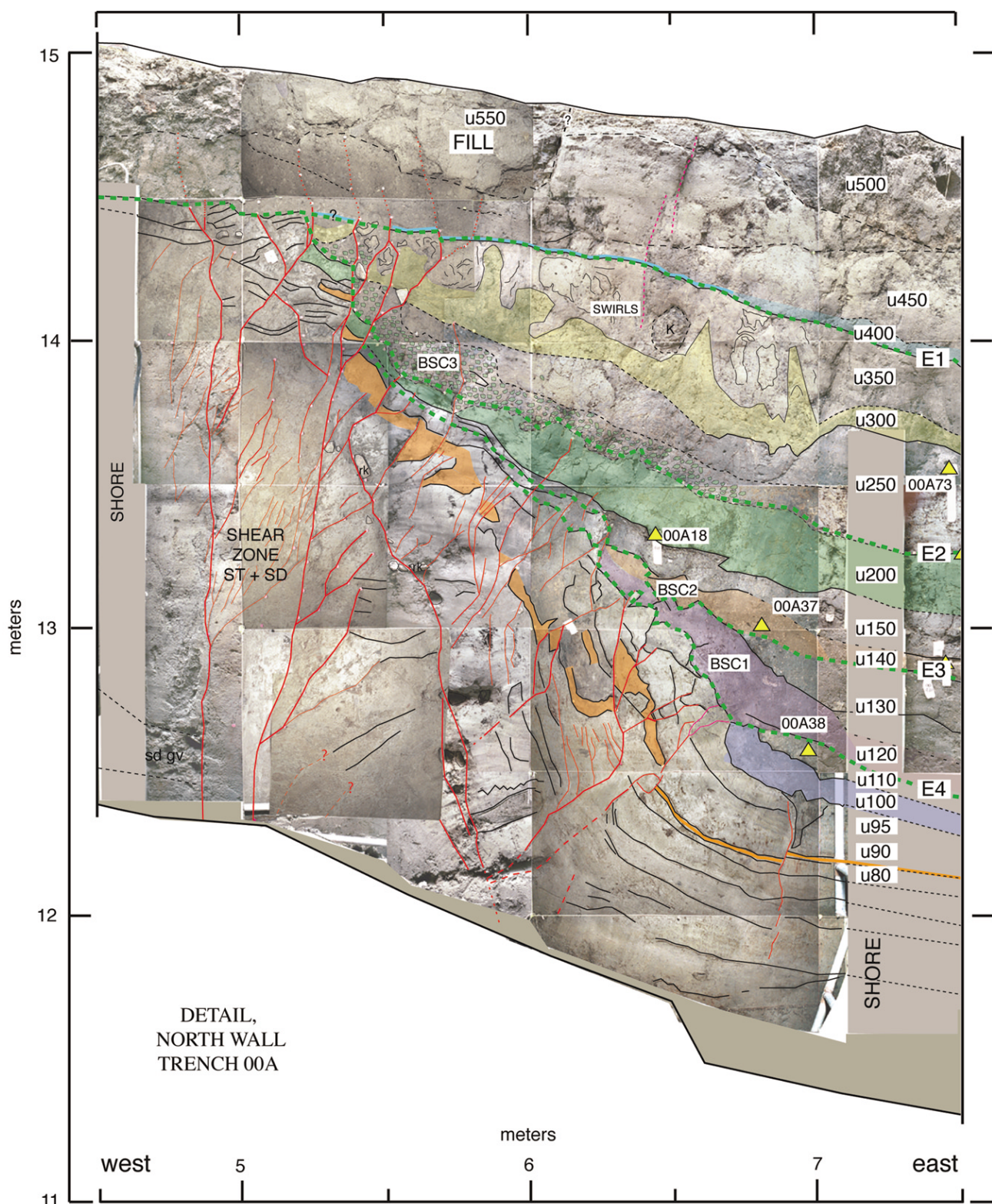


Figure 7. Enlargement of main fault trace on the north wall of trench 00A.

of postevent scarp retreat related to rapid coseismic uplift and subsequent erosion across a fault with 3 m of vertical displacement. They also noted an absence of colluvial wedges on the downthrown side of the fault and a relatively continuous and uniform increase in deformation across the fault of progressively older stratigraphic units. Although the trenches are located in a volcanic tectonic setting on the flanks of Mt. Etna, the underlying driving mechanism of faulting should be irrelevant for identifying trench-scale features of event evidence across a fault. Based on these observations, Ferrelly *et al.* (2002) concluded that coseismic faulting and quasi-continuous creep produce different and distinctive sedimentary signatures in the stratigraphic record.

We consider the strongest evidence for paleoearthquakes to be the existence of packages of blocky scarp colluvium deposited adjacent to the main fault trace (Fig. 8). In contrast to other lines of paleoseismic evidence, the formation of blocky colluvium appears unique to coseismic ruptures because the blocks of sediment must be shed off a newly exposed fault scarp relatively quickly. We are unaware of a process that may generate such colluvium through creep alone. The genesis of such deposits is proposed in Figure 8, and support for such a model comes from our following descriptions of particular events. We describe the evidence for the occurrence of four ground-rupturing earthquakes during the past 500 yr and summarize this evidence in Table 1. The inferred ground surfaces (event horizons) at the time of each event (E1, E2, E3, E4) are shown in the logs (Figs. 4–7) as dashed green lines. Unlike the main trace, the eastern fault zone in trench 00A lacks identifiable packages of blocky scarp colluvium that would serve as strong evidence for coseismic ruptures. However, this fault zone does express upward terminations and abrupt changes in the amounts of deformation at the same stratigraphic horizons where we have identified events at the main trace. Although this would not be considered conclusive evidence for paleoearthquakes in itself, we consider it highly corroborative evidence for coseismic rupture when combined with our observations at the main trace.

Event E1 (1868 Earthquake)

We interpret the most recent event (MRE), E1, to be the M 6.9, 1868 earthquake. This event is known to have ruptured through Tyson's Lagoon and was apparently accompanied by liquefaction in the pond. Lawson (1908, p. 443) described the rupture of the 1868 earthquake at Tyson's Lagoon: "The lagoon parted lengthwise down the middle and threw water and mud both ways." We interpret the widespread swirling and mixing of units u350 and u300 (also seen in trenches 00B and 00C) as the stratigraphic manifestation of the liquefaction described by Lawson after the 1868 event. The overlying u400 organic clay is only slightly offset, presumably from creep, so the 1868 event horizon is at the contact between u350 and u400. The deformation of units u350 and u300 is most intense near the main fault where these swirled units thicken east of the fault zone (near

meters 5–7, Figs. 4–7). These units may have flowed off the upthrown side of the fault. Additionally, units deformed only by E1 (u300 and u350) are distinctly less deformed than units deformed by earlier events. Evidence for E1 is strengthened by the historical age of this event horizon (discussed in next section) and documentation of rupture at this location by Lawson (1908).

Event E2

Our best evidence of event E2 is the presence of an about 0.3-m-thick, blocky scarp colluvium (BSC3). This colluvium is composed of clay clasts derived from unit u200 in a silty sand matrix, which is draped over the main fault (Figs. 4–7). This deposit appears to have been produced by mixing of clay fragments of unit u200 with a matrix of sand and silt derived from the underlying sand and silt deposits west of the main fault. The lack of liquefaction suggests that the pond was dry at the time of the earthquake. The E2 event horizon is also marked by upward terminations (near meters 5–6, Figs. 4–7) and abrupt changes in the degree of warping of older and younger units (near meter 5 and meter 11, Figs. 4–7).

Event E3

Evidence for event E3 also includes a blocky scarp colluvium (BSC2). This colluvium is an approximately 0.2-m-thick package composed mainly of blocks of the underlying shell-rich unit u130. Its matrix is composed of comminuted clasts of unit u130 that abuts the main fault zone (near meters 6–7, Figs. 4–7). The fault scarp is a complex shear zone of many strands, but the boundary between the complexly sheared zone to the west and unit BSC2 is distinct and near vertical. Additional evidence of event E3 is expressed as soft-sediment deformation (liquefaction) of swirled ash layers, unit u135, (meters 9–10, Fig. 5), presumably caused by earthquake shaking. Unit u140, which immediately overlies u135, consists of similar sediments and is not liquefied, which suggests that the event horizon for E3 is located at the contact between these two units.

Event E4

Event E4 is the most strongly expressed event in our trenches. It produced an approximately 0.45-m-thick blocky scarp colluvium unit, BSC1. This colluvium is distinguished from the overlying BSC2 by being composed entirely of blocks of gray clay (unit u110) that tumbled from the scarp during E4. It contains none of the abundant shells found in the overlying unit BSC2 and u130. Many fault strands terminate at E4 on the antithetic fault (near meters 10–11, Figs. 4, 5) and the event horizon is marked by abrupt changes in degree of warping (near meters 5–7 and meters 10–11, Figs. 4–7).

Evidence for earlier events is much weaker than for events E1, E2, E3, and E4. Equivocal evidence exists for an earlier event in the form of possible fissure fills that include clasts of u100 and extend below unit u100 (near meter 10

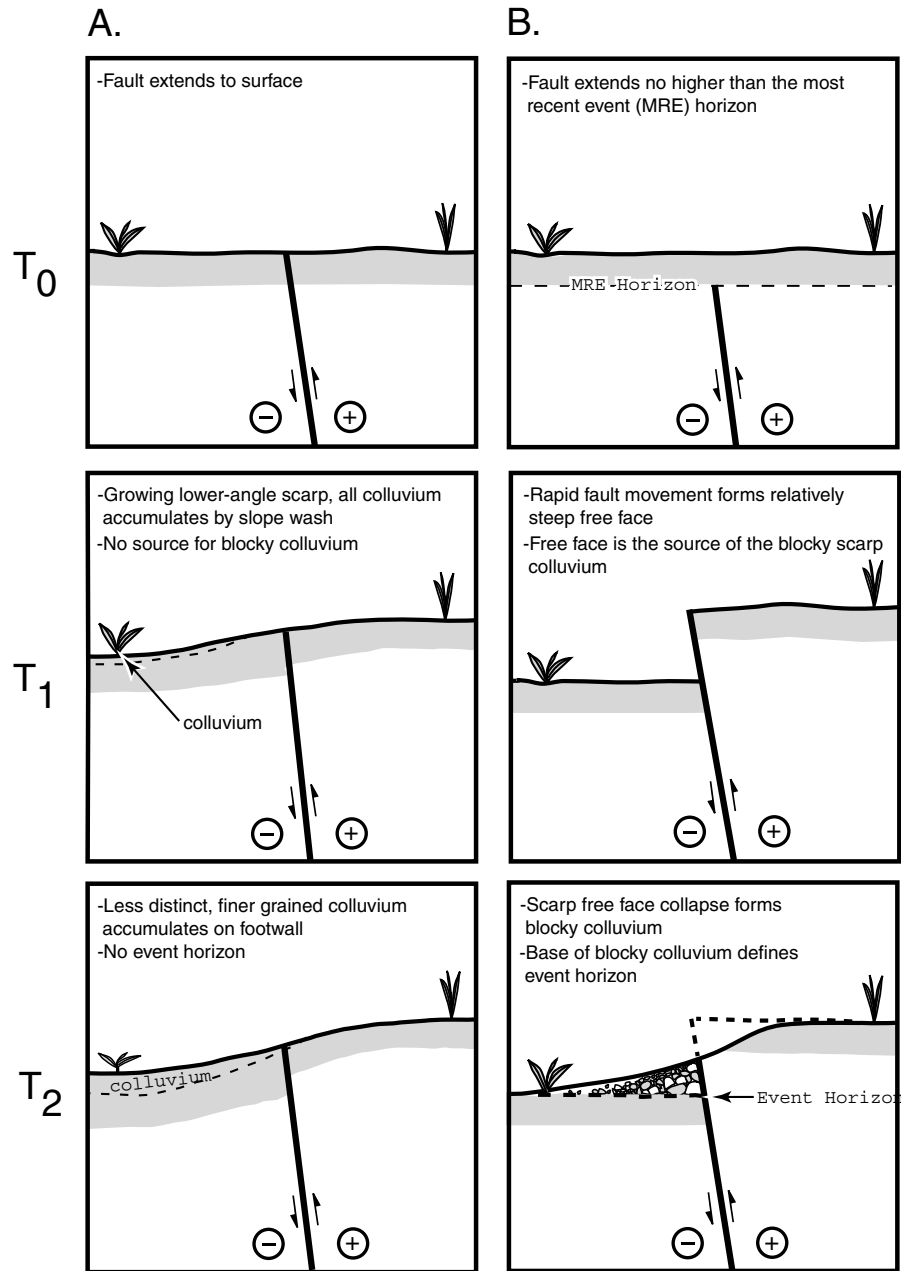


Figure 8. Diagram contrasting the formation of an oblique-slip fault scarp, produced (A) by creep alone versus (B) by coseismic slip alone. Gray pattern indicates surficial layer. (A) Sketches on left show gradual growth of scarp through time on a fault that moves exclusively by steady creep. (B) The sketch on the right shows absence of scarp before rupture (T_0), coseismic uplift during fault rupture (T_1) and development of scarp colluvium following rupture (T_2). Plus/minus signs indicate sense of strike-slip movement.

on Fig. 4 and near meter 7 on Fig. 7). However, no other features of coseismic origin are associated with this stratigraphic level, so these features may more likely represent root casts or krotovina. Stronger evidence of an even earlier event is expressed as upward terminations (meters 10–11, Fig. 5) and contrast in degree of deformation in the main fault zone (near meters 5–6.5, Fig. 4–7). However, in both

cases the evidence for and dating of these earlier possible events is less certain than for the four youngest events described previously. In addition, sedimentation rates are much lower in the lower part of the trench, which makes complete recognition of events difficult or impossible. Because of this uncertainty, we concentrated our dating efforts (see below) on obtaining ages of the four youngest events.

Table 1
Summary of Evidence for Paleoearthquakes

Event Horizon	Blocky Scarp Colluvium	Upward Terminations	Much Less Deformation Above	Liquefaction	Notes
E1	—	—	Yes	Widespread	U300 and u350 thickened near scarp by partial liquefaction
E2	Yes-BSC3	Several	Yes	—	Clay clasts of u200 from scarp in BSC3
E3	Yes-BSC2	—	Yes	Yes (u135)	Blocks include shells of u130 in BSC2
E4	Yes-BSC1	Several	Yes	—	Blocks of gray silt, no shells in BSC1

Earthquake Chronology

Chronological constraints on the age of four earthquake horizons (E1, E2, E3 and E4) come from the historical earthquake record, human settlement in the region, the first occurrence of nonnative pollen, and radiocarbon dating. We first describe each of these types of data separately. Then we describe a chronological probability model, which integrates all of these data and their uncertainties to produce estimates of the ages of the events, the intervals between them and the mean recurrence interval.

Historical Constraints

The youngest constraint in our earthquake chronology is the known occurrence of the 1868 earthquake on the southern Hayward fault, which we correlate to the MRE (E1) event horizon. A second historical constraint is that no other major earthquakes has been associated with the southern Hayward fault during the historical period, that is, since the first settlement in San Francisco in A.D. 1776. However, early settlement was sparse and the first settlement near the Hayward fault was the establishment in A.D. 1797 of Mission San Jose in Fremont. Therefore, there is a slight possibility that a large surface-rupturing earthquake on the Hayward fault might escape mention in the period A.D. 1776–1797. These historical data can be related to the appearance of the first nonnative pollen (*Erodium cicutarium*), which approximately coincides with the arrival of the Spanish in A.D. 1776 (Mensing and Byrne, 1998). Although, no precise record is available for the San Francisco Bay region, pollen of *E. cicutarium* has been identified and its first arrival precisely dated in the Santa Barbara area. There this pollen was shown to have preceded local Spanish settlement through rapid natural propagation by as much as 20 yr (Mensing and Byrne, 1998). In trench 00A, the first appearance of the non-native pollen *E. cicutarium* is at the base of unit u250 (Lienkaemper *et al.* 2002).

We combine the age constraints from the pollen and historical earthquake record to approximate an age of A.D. 1780 ± 20 yr for this stratigraphic position (i.e., base of u250). We derive this age and its error limits from the historical constraints described previously. Our best estimate of nonnative pollen arrival is coincident with the arrival of Spanish settlers in San Francisco in A.D. 1776, which we round to the nearest decade (1780). Our older age limit (-20

yr) is based on the rates of natural pollen propagation in the Santa Barbara area (Mensing and Byrne, 1998). Our younger age limit ($+20$ yr) is based on a lag of about 20 yr in the date of settlement and establishment of historical records in Fremont.

Radiocarbon Constraints

Chronological control is based primarily on 51 accelerator mass spectrometry (AMS), radiocarbon-dated samples from 14 stratigraphic levels in trench 00A and 00B. The radiocarbon-dated samples consisted of 25 detrital charcoal samples and seven associated humic acid extractions, one plant fiber and an associated humic acid extraction, one seed sample, six shell, and 10 soil fungus samples. Because chronologies based solely on detrital samples have inherit limitations of context uncertainty, we explored the usefulness of dating other materials in this sag pond environment, which is typical of many paleoseismic sites. The field sampling and near real-time laboratory analysis were coordinated to assure a seamless integration of these tasks, which too often are separated, diminishing the quality of results. Analysis was performed on this variety of samples to provide insight into the source, transport, and sedimentation processes. Ultimately, an understanding of these processes helps assess how representative the ^{14}C age determinations are of the depositional ages.

Laboratory Pretreatment

All samples were examined under a 40-power microscope to determine sample origin, which proved to be a critical task, because the soil fungus samples would otherwise have been mistaken for weathered detrital charcoal. In sediments, various mobile carbon fractions exist, which have the potential to become attached to radiocarbon samples. Various forms of physical and chemical pretreatment are applied to the samples, which strongly affect the ^{14}C content. In theory, the fractions can be separated, however in all practicality, the pretreatment methods are a compromise between removing the undesirable carbon fraction (commonly considered contamination), and not eliminating the desired carbon fraction. The standard pretreatment of charcoal consists of an acid wash to remove absorbed fulvic acids, followed by an alkali wash to remove absorbed humic acids. Both the fulvic and humic acids are generally considered possible contaminants of the charcoal and hence are routinely dis-

carded. The dating of the extracted carbon fractions from individual, detrital charcoal pieces has become feasible with the greatly reduced, minimum sample-size requirement of the AMS radiocarbon method, from about 1 g C for counting methods to 0.05 mg C by AMS.

Context Uncertainty and Sample Selection

There are two main sources of ^{14}C dating uncertainty: context and analytical (McCalpin and Nelson, 1996). The context uncertainty is the difference in age between the event of interest and the sample age. In our case this uncertainty is due to the detrital source of most samples and generally greatly exceeds the analytical uncertainties. The analytical uncertainty is associated with the counting statistics of the AMS operation, which increases with age and when the sample size is smaller than the optimal 1 mg of carbon. The analytical variations in our results are associated mainly with sample size. Three evaluation criteria were used to assess which samples provide the most representative layer age estimates and hence were selected for chronological modeling. First, the sample ages must follow stratigraphic order. Second, the samples ages must be consistent with historical age constraints. Lastly, we considered how well particular types of sample materials provide reliable ages. These criteria were applied to all dated samples and considered in their geologic context before samples were selected for chronological modeling.

A scatter plot of ^{14}C age versus sample depth and stratigraphic level (Figs. 9, 10) was used to identify which samples and sample types provide reliable estimates of the layer age. It is useful to focus on the pattern of all ages, of sample material types, and the variation of ages within individual layers. A stratigraphically consistent relationship of depth versus increasing age can be represented by a line, which connects the youngest ages from each level. The resulting line forms a margin along the left side of the data points (dashed line, Fig. 10). We interpret the older scatter of ages to be the result of reworking of charcoal from older sediments, combined with the incorporation of burned originally older wood. Both processes are common in this depositional environment. Reworking of charcoal was likely enhanced by coseismic exposure of older sediments in the fault scarps bounding the graben. It should be noted that the x -axis of Figures 9 and 10 is in ^{14}C -years, which do not correspond directly to calendar years. The cluster and possible reversal of ages within the section near 2-m depth appears to be associated with the observed reversals in abundance of atmospheric ^{14}C (Stuiver *et al.*, 1998). We use this plot to illustrate our sample selection for the chronological model, though we did consider the magnitude of ^{14}C reversals of up to 125 ^{14}C -years in the past 300 yr. For example, the AD 1780 pollen/historical calendar year constraint is interpreted to fall essentially on the peak of a ^{14}C reversal at 220 ^{14}C -years, which drops to 90 ^{14}C -years at A.D. 1700. Radiocarbon calibration is integrated into the model calculations described later (Stuiver *et al.*, 1998).

We also considered the possibility of an older depth-versus-age relationship, which trends through or along an older margin to the right of the data. However, if such an older depth-versus-age relationship were real, it would necessitate pervasive postdepositional addition of younger organic matter, down-section across multiple stratigraphic layers. Although inclusion of younger material (rejuvenation) has occurred at the site, the following lines of evidence indicate that we avoided sampling such materials. First, the pattern of age results allows us to recognize a clear younger bound of ages that exhibit stratigraphic consistency. If rejuvenation were pervasive then a shotgun pattern of ages would be expected. Secondly, we include in our analysis a sufficiently large number of samples of various materials that would greatly facilitate the recognition of a widespread rejuvenation effect. Lastly, the excellent stratigraphy allows the recognition of most krotovina (infilled burrows), which we avoided for sampling.

We recognized two forms of bioturbation as possible younger contamination processes. The first form extends to greater depths affecting multiple layers, including the burrowing of ground squirrels and intrusive roots. The second form is shallow, within-layer mixing due to smaller scale animal and plant bioturbation. Fortunately, it appears that the chronologically more-problematic processes that result in introduction of younger material downward across multiple layers occurred less in the lower part of the exposed section than we observed in the more recent layers near the surface. This interpretation is consistent with the generally sharp layer contacts and presence of shell-rich layers in the lower section. Both suggest that standing water or a near-surface groundwater table was the dominant condition at the site in the past, which would tend to restrict penetration by deeply burrowing animals and large roots. Furthermore, the subsidence of the graben would have facilitated the preservation of these layers if they were dropped below the water table. All of the samples that we consider reliable and use in our chronological model were taken from the graben. We sampled where sedimentary structure was evident and free of such deep bioturbation. The shallow, within-layer-mixing process appears to have had little or no impact on our ^{14}C chronologies, because most individual layers span relatively short times. One possible exception is unit u100, which appears to span 200–300 yr based on ages of a burn layer and seeds.

The use of radiocarbon ages from humic acids extracted from detrital charcoal for determining chronologies is uncommon and requires considerations different from detrital charcoal (see discussion in Appendix 2). Based on empirical evidence from this site, we infer that these humic ages provide reliable estimates of the depositional ages of layers at this site. Although our experimental humic acid ages appear to be reliable, we tested our chronological model both with and without inclusion of humic acid ages. Radiocarbon ages on soil fungus and shells are more problematic (Appendix

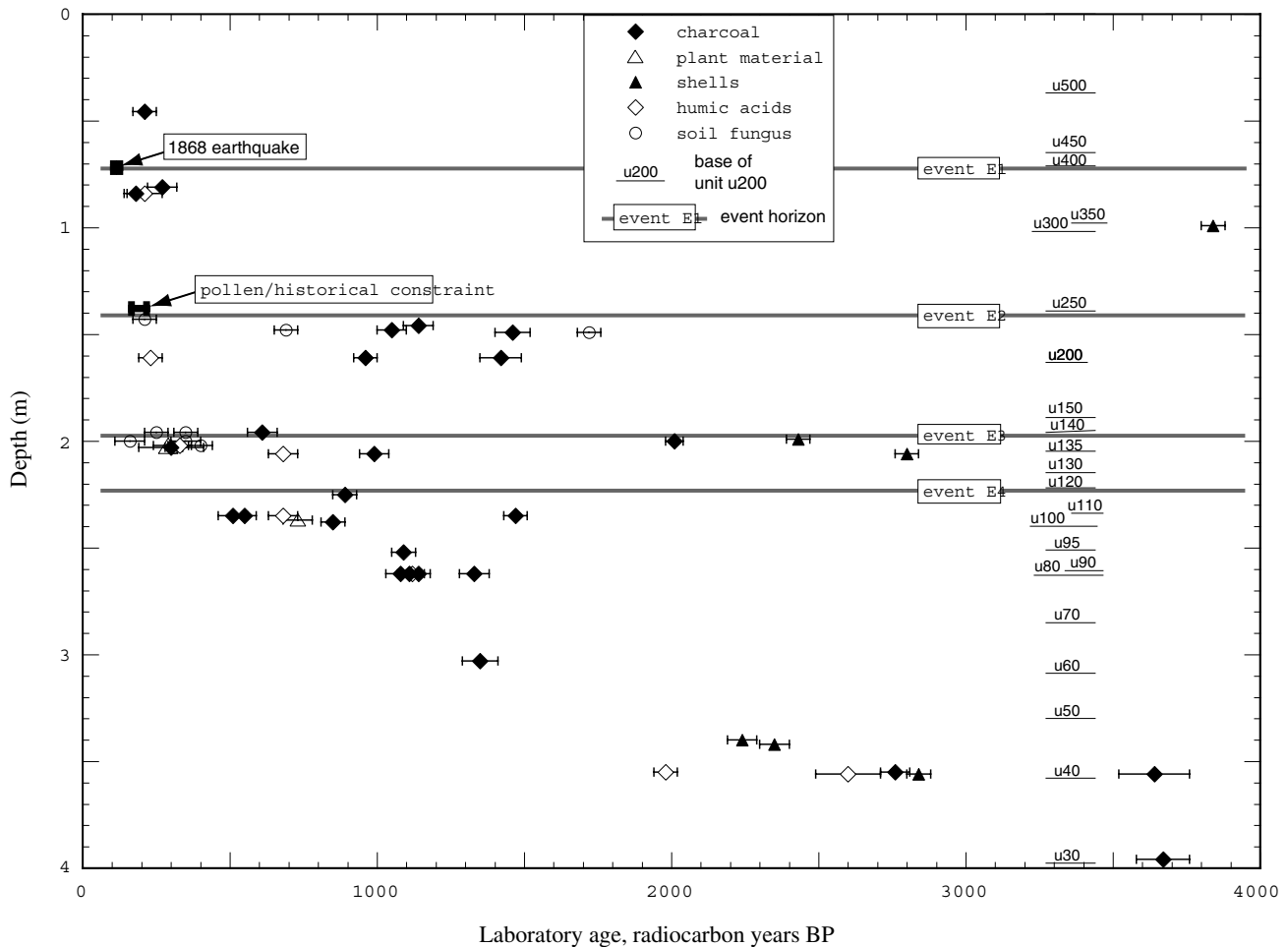


Figure 9. Scatter plot of uncalibrated radiocarbon ages ($\pm 1\sigma$) versus stratigraphic sequence by depth below the ground surface. Positions of event horizons relative to the stratigraphic levels are shown as gray lines labeled E1, E2, E3, and E4. Historical constraints, ranges shown as heavy error bars, are derived by converting historical dates to their equivalent in radiocarbon years (P. J. Reimer, personal comm., 2002). Depths of samples plotted normalized to a section located at the pollen sampling location (meter 8, south wall, Fig. 4). For location of older units outside the graben, u30 to u80, see Lienkaemper *et al.* (2002).

2) and have not been used in our modeling of the earthquake chronology.

In summary, our data analysis, with a focus on the sample origin and the possible pathways of incorporation into the sedimentary sequence, provides a basis for sample selection used in chronological modeling. The overall pattern of dating results is consistent with the geologic observations. We have identified the reworking of detrital samples as the dominant cause of the scatter in older ages. Although we considered an alternative age model involving the postdepositional addition of younger material through bioturbation, we have no evidence that it affected our results. Our proposed age model is consistent with the age estimates of the three stratigraphic levels for which we have the highest relative confidence. These stratigraphic levels are the two historically dated layers and ^{14}C -dated unit u100 below event

E4, which contains the samples in which we have the greatest confidence. We selected the youngest credible samples (detrital charcoal, plant material and one humic acid) from each layer for the chronological model. These samples provide a depth-age relationship that is consistent with the observed geologic conditions and the independent, historical constraints at two well-defined stratigraphic levels.

Chronological Model

We constructed a chronological model using the Bayesian statistical computer program Oxcal (Ramsey, 2000) as a means of incorporating all available chronological constraints. When radiocarbon ages are calibrated to calendar ages, the results can be expressed as probability distributions, which are often irregular and multimodal as shown in Figure 10 (Stuiver *et al.*, 1998). These distributions can be

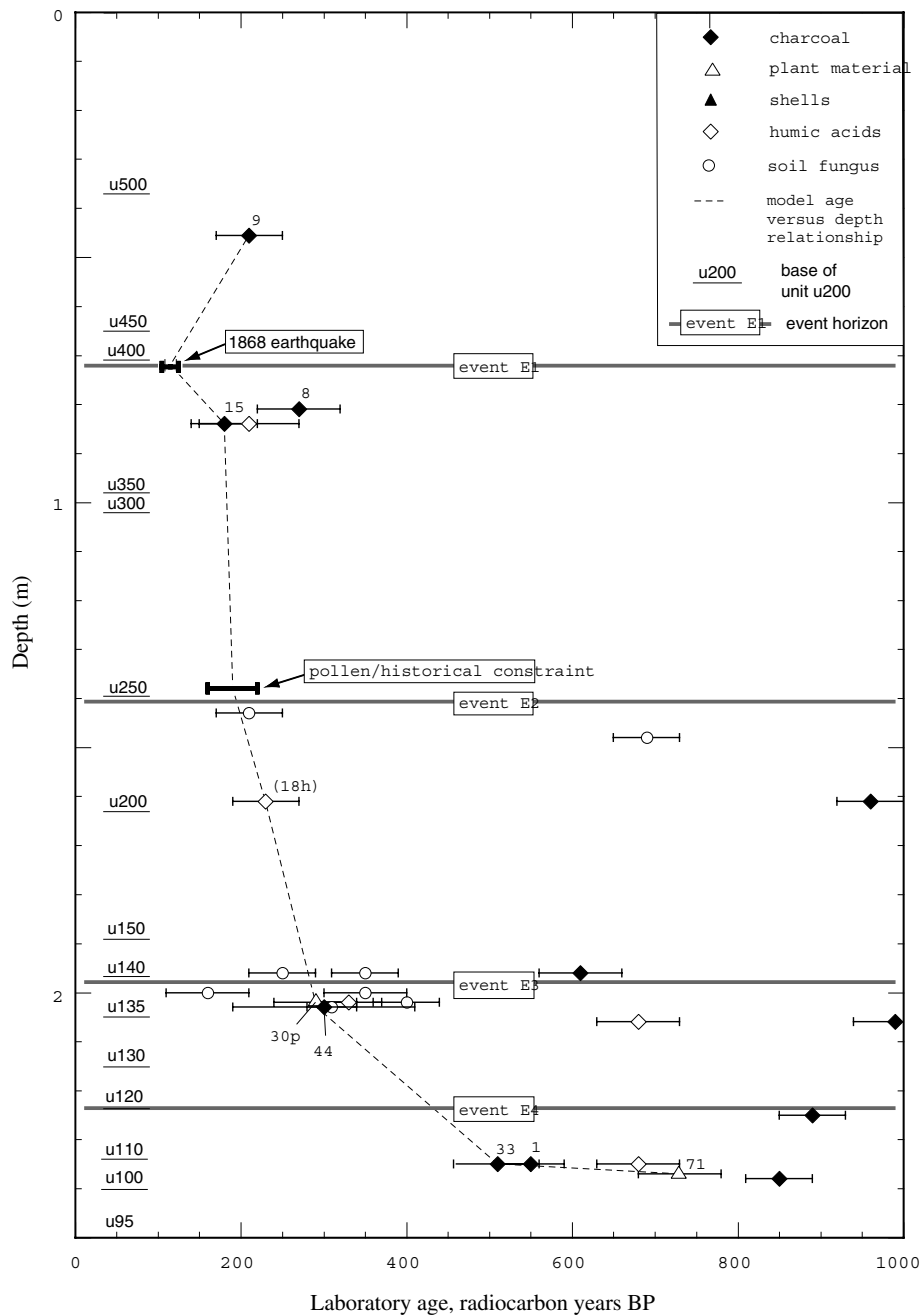


Figure 10. Expanded scatter plot of laboratory radiocarbon age ($\pm 1\sigma$) versus depth for past 1000 radiocarbon years BP. Dashed line approximates the age versus depth relationship in chronological model. Sample numbers shown are those included in the chronological model.

improved by including additional chronological information. Stratigraphic order, the timing of the most recent event, and historical constraints are inputs into the model. Applying the stratigraphic order as a constraint is particularly powerful where calibrated age distributions overlap, in which case the modeling calculations reweight the distributions to reflect the knowledge that overlying layers must be younger.

We use the results of our Bayesian Oxcal model, shown in Figure 11, to constrain the ages of the past four earth-

quakes (E1, E2, E3, and E4). The youngest event E1 is the 1868 earthquake, as confirmed by the historic and pollen data described previously. Two ages on charcoal (00A8 and 00A15) and one on humic acids (00A15h) are consistent with this result (Fig. 10). Event E2 is older than both non-native pollen introduction and the local historic record, A.D. 1780 ± 20 yr. The lower chronological constraint for E2 depends on a sample of humic acids extracted from charcoal (sample 00A18h), which implies that the six ages on detrital

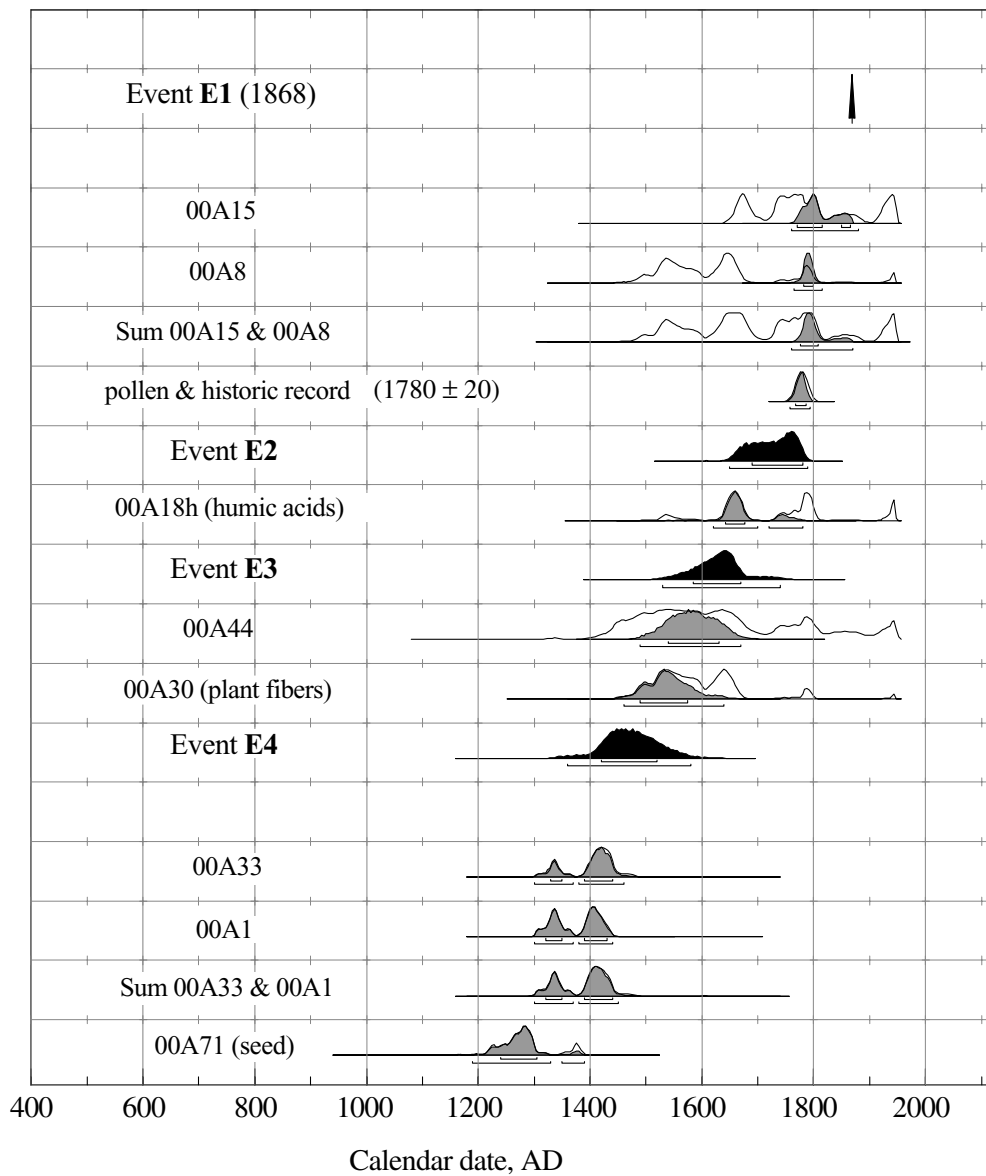


Figure 11. Bayesian model of constraints on timing of paleoearthquakes (using OxCal, Ver. 3.5) (Ramsey, 2000). Outlines show probability distributions of calibrated radiocarbon ages of samples and groups of samples prior to running the model. Gray areas show limits placed upon these distributions by the other age constraints including historical knowledge of the 1868 earthquakes and the onset of nonnative pollen circa A.D. 1776 (1780 ± 20 yr). Black areas represent probability distributions inferred for the paleoearthquakes. Lines below each distribution show limits of the 95.4- and 68.2-percentile confidence ranges for these samples and events. Sample material is detrital charcoal except where noted.

charcoal from this stratigraphic level must be too old (Table A1). Sample 00A18h gives the only age from this stratigraphic level that fits both the historic constraints above and the age of 500–700 ^{14}C -years from the well-determined ages near the base of our paleoearthquake sequence (i.e., unit u100). The resulting age range with sample 00A18h for E2 is A.D. 1650–1790. To test the stability and sensitivity of our model, we made several alternative runs of the Oxcal program for the E2–E3 interval. These alternative runs in-

cluded (1) deleting sample 00A18h from the chronology and (2) substituting an assumed 50-yr minimum sedimentation time for the E2–E3 interval. All three Oxcal runs yielded similar results, so for simplicity of discussion we present results for event ages and intervals based on the model using the humic acids (00A18h) sample.

Unfortunately, the upper stratigraphic constraints for event E3 are the lower constraints for E2, so the precise timing of this event is also less well known. The lower con-

straint for E3 is from an age on a sample of plant fibers (sample 00A30p). We were unable to identify the type of plant matter comprising this sample, so it is possible that this is a sample of decomposed root. However, a second age on a small piece of detrital charcoal (sample 00A44), possibly from a partially liquefied, *in situ* burn layer, yielded a nearly identical age, thus corroborating the validity of sample 00A30p. The resulting age range for E3 is A.D. 1530–1740. The lower age bound of event E4 is well constrained, because many samples give a consistent age from underlying unit u100. It contains unburned seeds from lower in the horizon and abundant charcoal from a major burn layer on the surface of the horizon. This unit (u100) most likely formed during a two to three hundred year period, which included one or more burns at the site. The resulting age range for E4 is A.D. 1360–1580.

Until this point, we have not expressed any central values (e.g., means) for the age of E2, E3, and E4, because important caveats must first be expressed about their reliability. Mean ages depend to some considerable but unknown degree on context issues such as how closely the ages of samples reflect the ages of deposition and how closely the suite of samples brackets each event. With improved sampling, mean ages could change considerably, but we expect them to remain with the calculated 95-percentile ranges of uncertainty. Given these caveats, the mean ages of E2, E3, and E4 (and 95-percentile ranges) are A.D. 1730 (1650–1790), A.D. 1630 (1530–1740), and A.D. 1470 (AD 1360–1580), respectively.

Recurrence Intervals

The recurrence intervals defined by our chronological results have considerable importance in understanding the long-term behavior of the southern Hayward fault and its potential seismic hazard. The individual modeled recurrence intervals are $140 + 80/-70$ yr (E1–E2), $100 + 90/-100$ yr (E2–E3), and $150 + 130/-110$ yr (E3–E4) and have large (95 percentile) errors that reflect the error ranges of the age determinations (Figs. 11, 12). These error estimates in the age of individual events are considerably larger than the 40-yr error derived to estimate the mean itself (130 ± 40 yr) using the overall age constraints for the past four events. This distinction may be significant when applying such data to a seismic hazard model.

Discussion

In the previous sections, we present evidence for the occurrence and timing of the past four surface-rupturing earthquakes at the Tule Pond site on the southern Hayward fault. A major objective of paleoseismic studies is the development of an understanding of the behavior of faults in time and space. Ideally, this understanding is based on observations at multiple localities along the length of a fault. We do not have this luxury with the Hayward fault. However, the occurrence of four surface-faulting earthquakes

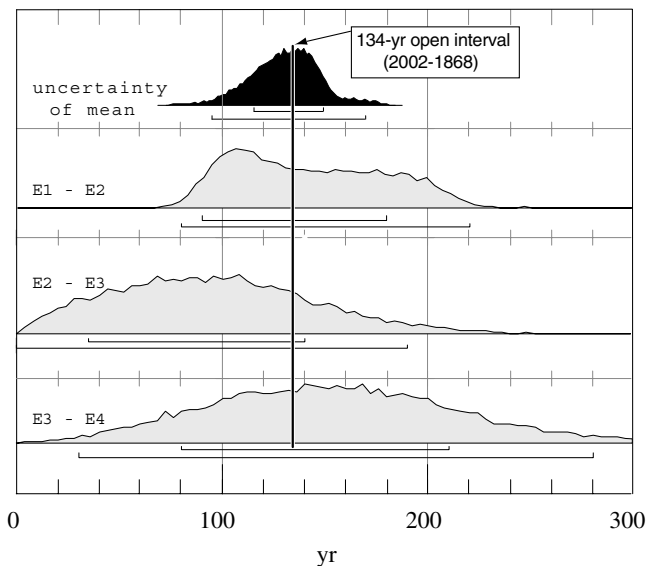


Figure 12. Probability distributions of the individual, modeled recurrence intervals (E1–E2, E2–E3, E3–E4) and average of these distributions. Brackets below distributions indicate 95.4- and 68.2-percentile confidence ranges. Uncertainty of the mean here depends on the uncertainty in the age of E4, where mean is computed as the average of three intervals from A.D. 1470 ± 110 yr to 1868. The 134-yr open interval since the most recent earthquake in 1868 is shown as a vertical line for comparison to the mean and observed intervals. Although the 130-yr mean interval is well determined, it is important to note that the three previous intervals may have been much longer or shorter than the mean.

since A.D. 1360, with a relatively short mean recurrence interval of 130 ± 40 yr, raises questions about the southern Hayward fault in terms of its basic behavior and the associated hazard. In the following discussion, we examine alternative implications for the size of past earthquakes and slip rate on the Hayward fault in the context of several other observations and interpretations. These are the effect of the 1868 rupture on deposits in the Tule Pond trench, the estimates of rupture length and average slip as modeled geodetically for the 1868 earthquake (Yu and Segall, 1996), and Holocene slip rates (Lienkaemper and Borchardt, 1996).

Earthquake Size

The size or magnitude of paleoearthquakes can be estimated from the amount of coseismic slip that has occurred during individual past events. For strike-slip faults, measurement of gully offsets at the surface or offset buried stream channels in trenches, especially at multiple sites, can be used to estimate the seismic moment of past earthquakes. These types of data are not available for the Hayward fault, due in large part to the effects of creep. Steady creep appears to attenuate coseismic surface rupture so that when it does occur, the resulting coseismic surface slip is significantly smaller than the slip at depth. No certain evidence of the

amount of coseismic dextral slip is available for the 1868 earthquake. Lawson (1908, p. 447) summarized the dextral slip as follows: "The amount of horizontal movement, if any, was much less than on the San Andreas fault in 1906, and its direction is unknown. In contradiction to this statement, Lawson (1908) described a few inches of distinctly right-lateral afterslip. In addition, Lawson describes a possible maximum slip of unknown direction or sense, ". . . a displacement of 3 feet [0.9 m] is said to have been observed." Lawson's observations were from eyewitness accounts of lay persons that were recorded forty years after the earthquake. In contrast, the geodetically modeled average slip for this event is 1.9 ± 0.4 m ($\pm 1\sigma$) (Yu and Segall, 1996), a value much larger than any known to have been observed at the surface. Both creep and coseismic slip contribute to surface offset, so that paleoseismically, even when a single-event piercing point is found, the ratio of coseismic slip to creep is uncertain. These complexities limit our ability to use surface offset measurements on creeping faults to estimate earthquake magnitude directly. However, in the case of the Hayward fault, we can associate vertical deformation inferred for the 1868 earthquake in the Tule Pond trench with independent estimates of the magnitude in 1868. These are M 7.0 estimated geodetically (Yu and Segall, 1996) and M 6.8 from intensity data (Bakun, 1999). A comparison (below) of the vertical deformation in 1868 provides an important observation for comparing its relative size to that of the three preceding earthquakes.

In the Tule pond trench, there were no piercing points that could be used to measure the amount of horizontal slip that occurred in each of the past four earthquakes. However, we were able to estimate amounts of repeated vertical slip on the main fault scarp. For the 1868 earthquake (E1), our best estimate of local vertical displacement is 0.1–0.2 m derived from vertical separation of unit u300. Local vertical slip from the earlier events is approximated from the thickness of blocky scarp colluvial deposits associated with each event. These are 0.3 m (E2), 0.2 m (E3), and 0.45 m (E4), values not dissimilar from 1868. Although the ratio of vertical-to-horizontal slip is not known here, a common observation on strike-slip faults is that locally it remains relatively constant. Taking into account uncertainties and assumptions, we find nothing in our analysis to suggest that coseismic surface slip at the Tule Pond during events E2, E3, and E4 was demonstrably different from that which occurred in 1868. What, then, does this imply about the magnitude of these past events?

Earthquake magnitude is controlled by the average slip and the area on the fault plane over which that slip occurs (Hanks and Kanamori, 1979; Wyss, 1979). Slip at the Tule pond represents only one point on the fault. Without repeated slip estimates at other locations it is uncertain how similar or different the slip distribution along strike, and therefore the average slip, was for the pre-1868 earthquakes. Yu and Segall (1996) modeled the 1868 earthquake using geodetic data as a 52-km-long rupture extending from south-

ern Fremont on the south to near Berkeley on the north. In fact, the 1868 rupture may have extended >60 km based on additional geologic information (Hayward Fault Paleoearthquake Group, 1999; Lienkaemper and Galehouse, 1998). Even with slip at the Tule Pond remaining essentially constant, the fault rupture lengths for the paleoearthquakes could have been shorter or longer than 1868.

With only the relative vertical slip at the Tule pond site as a guide, we cannot precisely estimate the magnitude of repeating earthquakes from the trench exposures alone. However, with the observations that show repeated similar vertical slip and the independent magnitude estimates of 1868 based on geodetic and intensity data, we can suggest that magnitudes of events E2, E3, and E4 were comparable to 1868. That is, they were likely near the M 6.8 to 7.0 range, although the uncertainties allow for specific magnitudes that are somewhat smaller or larger.

Earthquake Recurrence and Slip Rate

Our results suggest that the mean recurrence interval between large earthquakes that ruptured the surface at the Tule Pond site was 130 ± 40 yr during the past 500 yr. This mean of 130 yr is somewhat shorter than previous estimates, although earlier estimates were based on longer stratigraphic sequences or were calculated using fault segmentation models or slip rate and expected average slip per event. Williams (1993) estimated the southern Hayward fault's recurrence to be in the range of 150 to 250 yr during the past 2100 yr. That study had been the only published recurrence estimate for the southern Hayward based on identification of individual paleoearthquakes in trenches. The 1988 and 1990 Working Group on California Earthquake Probabilities (WG88 and WG90) estimated recurrence intervals on the southern Hayward fault of $209 [\pm 73]$ yr and 167 ± 67 yr, respectively. These intervals were calculated by dividing the expected slip per event (also a calculation) by the fault slip rate. In these estimates, the southern Hayward fault was considered an independent fault segment that failed in repeats of the same size earthquake. The most recent report of WG99 computed a recurrence interval of 160–360 yr in its model for the southern Hayward fault. The WG99 recurrence estimates resulted from a complex, geophysical model of the fault system and not from geological observations of paleoearthquakes. The model incorporated alternative rupture segment scenarios, the long-term fault slip rate, and the effects of fault creep. In contrast to the earlier calculations, WG99 recurrence is the mean rate of rupture of a range of earthquake sizes, M ≥ 6.7 , and includes earthquakes that not only nucleate on the southern Hayward fault but also nucleate on the northern Hayward fault or even the Rodgers Creek fault. Our study defines the mean rate of surface rupture at a single location on the southern Hayward fault during the past 500 yr. In this regard, our results are closer in meaning to the WG99 model in that they may reflect both southern-Hayward-only and multiple segment ruptures.

An important observation is that previous recurrence

estimates are longer than our results. There are several possible reasons for this shorter recurrence interval, which could have some significant physical implications. The model-based calculated intervals, such as those of the Working Groups (WG88, WG90, WG99), conceptually represent the long-term (Holocene) average behavior of the Hayward fault. In contrast, our paleoseismic recurrence is based on a small sample of four events and three intervals in a relatively short time, a maximum period of A.D. 1370–1868. With any long-term average, there is always the possibility of short-term variability. Earthquake clustering has become a popular concept and perhaps this is what our results indicate. On the other hand, the 130-yr mean interval from the Tule pond trenches may actually represent the longer-term recurrence interval for the fault.

Perhaps the most important physical implication of our recurrence interval regards the slip rate on the Hayward fault. The rate of 9 ± 2 mm/yr (WG90, WG99), which is based primarily on the offset of 4600- and 8300-yr-old buried channels (Lienkaemper and Borchardt, 1996), has been used for all seismic hazard analyses of the fault as well as for slip rate models of the Bay Area (WG88, WG90, WG99). Is it possible that shorter-term slip rates are higher? An important assumption is that large events, such as 1868, release the accumulated strain on the fault and reset the recurrence clock. In the Tule Pond trench, the oldest identified event is E4. The interval before E4 is unknown, so E4 becomes the initial resetting earthquake. Following E4, slip accumulated along the fault during E3, E2, and 1868. If the 1.9 ± 0.4 m mean, coseismic slip in 1868 estimated geodetically by Yu and Segall (1996) is characteristic of the paleoearthquakes in the Tule pond trench, then 5.7 m of slip accumulated and was released after E4. Based on our radiocarbon dating, the maximum interval in which this 5.7-slip could have occurred was A.D. 1370 to 1868, yielding a minimum slip rate of 11.4 mm/yr. Using the mean date of A.D. 1470 for E4 increases the rate to 14.3 mm/yr. Alternatively, the post-E4 slip rate could be the long-term rate of 9 mm/yr. In this case, the modeled 1.9-m average slip in 1868 may overestimate the actual 1868 magnitude, and earlier events might also have been smaller and thus had smaller average displacements. For example, although Yu and Segall (1996) estimated a magnitude from geodetic moment of **M** 7.0 for the 1868 event, Bakun (1999), used intensity data to estimate **M** 6.8, which is consistent with a lower coseismic slip of ~ 1 meter.

The possibilities discussed above are permitted within the uncertainties of the present modeling and observations. Only additional data will allow us to better constrain or choose between the alternatives. As noted, the interval for the earthquake chronology presented here is short, only the past 500 yr. The Tule Pond site contains older stratigraphy and as Williams (1993) has shown there is evidence of individual events extending back about 2100 yr. If a complete chronology of large earthquakes can be obtained for this longer interval at the Tule Pond, it will be possible to place the 130-yr mean recurrence for the past three intervals into

a broader context and evaluate whether it represents (1) a recent cluster or short-term increase in the rate of activity of the Hayward fault or (2) is characteristic of its longer-term behavior.

Regardless of the questions surrounding long-term versus short-term rates of recurrence and slip, we are confident in the reliability of the multiple lines of evidence for three paleoearthquakes (E2–E4) and the 1868 event in the trenches and of the 500-yr radiocarbon constraints on our mean recurrence. The mean recurrence interval of 130 ± 40 yr for the past three intervals is the major result of the present study.

Insights Gained from Chronologic Modeling

The results of our trenching and dating efforts may have important implications for other paleoseismic investigations. We based our chronology on an extensive suite of AMS ages on detrital charcoal, shells, extracted humic acids, and aggregates of soil fungus. Our results indicate that most detrital charcoal samples, and all shell samples, yielded ages too old, in some cases by hundreds of years. Had we relied on fewer samples and fewer types of samples, we would have biased our results toward older ages. Our most representative charcoal samples were those taken from interpreted *in situ* burn layers, which were not found at all stratigraphic levels. Although still experimental, ages on humic acids extracted from charcoal samples yielded promising results that may be applicable to studies in similar depositional environments. Our soil fungus results, which are also experimental, may also provide age constraints with a better understanding of their origin. In the meantime, geologists should be wary of dating any dull, black organic material resembling charcoal without first making a microscopic inspection of the sample.

This study demonstrates that chronological modeling that incorporates Bayesian statistics, greatly improves the results for the following reasons: It provides a method to incorporate additional information, including stratigraphic order and historical age estimates, such as the MRE. Incorporating more information is beneficial, because the influence of any single data point that might be inaccurate is diminished, while on the other hand, the overall consistency of the chronological data set is emphasized. Subjective chronological modeling decisions are minimized with this approach. The model is explicit and the influence of each input can be evaluated. This model approach facilitates a sensitivity analysis, which allows the recognition of the most influential data, such as the correlation of the uppermost event horizon with the MRE. Using other chronological information such as the time of first appearance of nonnative pollens can greatly improve the model, despite the limitations of ^{14}C -dating precision, especially during the past 300 yr.

Recognition of Paleoearthquakes on Creeping Faults

One of the contributions of this study is the identification of coseismic event evidence along a fault that experi-

ences both coseismic slip events as well as creep. In trench 00A, coseismic event evidence is best expressed as packages of scarp-derived blocky colluvium. For each event with an associated scarp-derived colluvium, we identify corroborating evidence in the form of upward terminations and abrupt changes in amounts of deformation. One question that arises is whether, in the absence of scarp-derived blocky colluvium, we would be able to identify paleoearthquakes in our trench. Ferrel *et al.* (2002) observed that on the rapidly creeping Pernicata fault, deformation of units across the fault was relatively continuous and uniform. In contrast, we observe abrupt changes in amounts of relative deformation as well as corroborating evidence in the form of upward terminations. For example, the secondary fault zone at meter 14–15 lacks scarp-derived blocky colluvium but does exhibit event evidence in the form of upward terminations and abrupt changes in the amounts of deformation. Furthermore, when put into the context of the chronologic model, we feel that it is extremely unlikely that the abrupt changes in amounts and character of deformation could occur within the short periods of time necessitated by the radiocarbon ages, because this would require the unlikely possibility of a sustained creep rate much larger than presently occurs. Also, we find it unlikely that upward terminations would form along a fault that is rapidly creeping. Instead, it is more likely that a creeping fault trace would be able to rejuvenate itself and cut younger sediments as they are being deposited, especially over time spans of a few hundred years. Our conclusion therefore is that in trenches lacking diagnostic evidence for coseismic slip event such as fissure fills and blocky scarp-derived colluvium, it is still possible to identify coseismic slip events along a fault that also experiences creep.

Conclusions

We present evidence for a record of four large earthquakes on the southern Hayward fault since A.D. 1470 \pm 110 yr with a mean recurrence interval of 130 \pm 40 yr (95-percentile uncertainty in the mean). Individual intervals are less well determined: E1–E2, 140 \pm 80/–70 yr; E2–E3, 100 \pm 90/–100 yr; and E3–E4, 150 \pm 130/–110 yr. Although we cannot determine the magnitudes of the three paleoearthquakes (E2, E3, and E4), local estimates of vertical slip suggest that these events were similar in size to the M 6.8–7.0, 1868 earthquake (E1). The mean recurrence interval of 130 \pm 40 yr is somewhat lower than has been determined or modeled in earlier work by others. More complete data for earlier recurrence intervals is needed to determine if a 130-yr mean recurrence reflects a short-term rate of occurrence or is representative of long-term behavior of the fault system.

Acknowledgments

The USGS National Earthquake Hazard Reduction Program (7460-09711) funded the investigation. We thank John Rogers of Alameda County Public Works Agency for making this work possible. We gratefully ac-

knowledge J. N. Alt for providing many unpublished details of his previous investigation of the site. Assistance with issues of statistics and chronological modeling from P. J. Reimer, P. A. Reasenberg, and G. P. Biasi is much appreciated. Further special thanks go to T. E. Fumal, H. D. Stenner, and two anonymous reviewers for their helpful reviews that improved this report.

References

- Bakun, W. H. (1999). Seismic activity of the San Francisco Bay region, *Bull. Seism. Soc. Am.* **89**, 764–784.
- California Department of Water Resources (1967). Evaluation of ground water resources: South Bay (Appendix A: Geology), *Calif. Dept. Water Res. Bull.* **118-1**, 153 pp.
- Ferrel, Luca, A. M. Michetti, L. Serva, and E. Vittori (2002). Stratigraphic evidence of coseismic faulting and aseismic fault creep from exploratory trenches at Mt. Etna volcano (Sicily, Italy), in *Ancient Seismites*, F. R. Ettenson, N. Rast, and C. E. Brett, (Editors), Geol. Soc. Am. Special Paper 359, 49–62.
- Frankel, A. D., C. S. Mueller, T. P. Barnhard, E. V. Leyendecker, R. L. Wesson, S. C. Harmsen, F. W. Klein, D. M. Perkins, N. C. Dickman, S. L. Hanson, and M. G. Hopper (2000). USGS National Seismic Hazard Maps, *Earthquake Spectra* **16**, 1–19.
- Hanks, T. C., and H. Kanamori (1979). A moment-magnitude scale, *J. Geophys. Res.* **84**, 2348–2350.
- Hay, E. A., N. T. Hall, and W. R. Cotton (1989). Rapid creep on the San Andreas fault at Bitterwater Valley, in *The San Andreas Transform Belt: 25th International Geological Congress Field Trip Guidebook T309*, A. G. Sylvester, and J. C. Crowell, (Editors), 36–39.
- Hayward Fault Paleoseismic Group (1999). Timing of paleoearthquakes on the northern Hayward fault, CA: preliminary evidence in El Cerrito, CA, U.S. Geol. Surv. Open-File Rep. OF 99-318, 33 pp. (<http://geopubs.wr.usgs.gov/open-file/of99-318>).
- Kelson, K. I., and J. N. Baldwin (2001). Can paleoseismologic techniques differentiate between aseismic creep a coseismic surface rupture? (abstract) *Seism. Res. Lett.* **72**, 263.
- Lawson, A. C. (1908). The earthquake of 1868, in *The California Earthquake of April 18, 1906*, Report of the State Earthquake Investigation Commission, Carnegie Institution of Washington Publication, Washington, D.C., Vol. 1, 434–448.
- Lienkaemper, J. J. (1992). Map of recently active traces of the Hayward Fault, Alameda and Contra Costa counties, California, U.S. Geol. Surv. Misc. Field Studies Map MF-2197, scale 1:24,000, 13 pp.
- Lienkaemper, J. J., and G. Borchardt (1996). Holocene slip rate of the Hayward fault at Union City, California, *J. Geophys. Res.* **101**, 6099–6108.
- Lienkaemper, J. J., and J. S. Galehouse (1998). New evidence doubles the seismic potential of the Hayward fault, *Seism. Res. Lett.* **69**, 519–523.
- Lienkaemper, J. J., T. E. Dawson, S. F. Personius, G. G. Seitz, L. M. Reidy, and D. P. Schwartz (2002). Logs and data from trenches across the Hayward fault at Tyson's Lagoon (Tule Pond), Fremont, Alameda County, California, U.S. Geol. Surv. Misc. Field Studies Map MF-2386, 2 sheets, 8 pp. (<http://geopubs.wr.usgs.gov/map-mf/mf2386>).
- Lienkaemper, J. J., J. S. Galehouse, and R. W. Simpson (2001). Long-term monitoring of creep rate along the Hayward fault and evidence for a lasting creep response to the 1989 Loma Prieta earthquake, *Geophys. Res. Lett.* **28**, 2265–2268.
- McCalpin, J. P., and A. R. Nelson (1996). Introduction to paleoseismology, in *Paleoseismology*, J. P. McCalpin, (Editor), Academic Press, San Diego, Chapter 1, 1–32.
- Mensing, S., and R. Byrne (1998). Pre-mission invasion of *Erodium cicutarium* in California, *J. Biogeogr.* **25**, 757–762.
- Ramsey, C. B. (2000). OxCal Program Ver. 3.5, Radiocarbon Accelerator Unit, University of Oxford, U.K. (http://units.ox.ac.uk/departments/rsla/orau/06_01.htm).

- Stenner, H. D., and K. Ueta (2000). Looking for evidence of large surface rupturing events on the rapidly creeping southern Calaveras fault, California, in *Active Fault Research for the New Millennium: Proceedings of the Hokudan International Symposium and School on Active Faulting*, K. Okumura, K. Takada, and H. Goto (Editors), Hokudan Co. Ltd., Hokudan, Hyogo, Japan, 479–486.
- Stuiver, M., and H. A. Pollach (1977). Discussion: Reporting of ^{14}C data, *Radiocarbon* **19**, 335–363.
- Stuiver, M., P. J. Reimer, T. F. Braziunas (1998). High-precision radiocarbon age calibration for terrestrial and marine samples, *Radiocarbon* **40**, 1127–1151.
- Williams, P. W. (1993). Geologic record of southern Hayward fault earthquakes, *Calif. Div. Mines Geol. Spec. Pub. 113*, 171–179.
- Woodward-Clyde and Associates (1970). Fremont Meadows active fault investigation and evaluation, Fremont, California, on file at California Division of Mines and Geology, San Francisco, California, file no. AP-744.
- Working Group on California Earthquake Probabilities (1988). Probabilities of large earthquakes occurring in California on the San Andreas fault, *U.S. Geol. Surv. Open-File Rept. 88-398*, 62 pp.
- Working Group on California Earthquake Probabilities (1990). Probabilities of large earthquakes occurring in the San Francisco Bay Region, California, *U.S. Geol. Surv. Circular 1053*, 51 pp.
- Working Group on California Earthquake Probabilities (1999). Earthquake probabilities in the San Francisco Bay Region: 2000–2030—a summary of findings, *U.S. Geol. Surv. Open-File Rept. 99-517*, 55 pp. (<http://geopubs.wr.usgs.gov/open-file/of99-517/>).
- Wyss, M. (1979). Estimating maximum expectable magnitude of earthquakes from fault dimensions, *Geology* **7**, 336–340.
- Yu, E., and P. Segall (1996). Slip in the 1868 Hayward earthquake from the analysis of historical triangulation data, *J. Geophys. Res.* **101**, 16,101–16,118.

Appendix 1

Stratigraphic Detail

Unit u80, an orange silty clay, is the lowest marker unit that could be clearly traced across the graben in trench 00A. It contains abundant charcoal and fire ash east of the graben. Overlying the orange silty clay are gray silty clays, units u90 and u95, identical except that unit u95 contains several fine charcoal stringers, the lowest of which forms the base of the unit. Above these gray clays is a black, organic silty clay, u100, colored by the abundant charcoal within it. Overlying the black clay is gray clayey silt, u110, which contains none of the gastropods that are abundant in three overlying units. Unit u120 is a silt with many gastropods that varies laterally in color from brown to gray. Near meter 8 (Figs. 4, 5), it overlies a blocky scarp colluvium, unit BSC1. The blocky scarp colluvial units are described in the section on evidence for paleoearthquakes. Overlying u120 is a similar unit, u130, differing mostly by a greater abundance of gastropods and generally a darker brown color. Both silt units u120 and u130 show considerable lateral variation in relative sand, clay, and organic content, and bioturbation has obscured much of the contact between them. Unit u135 is a dark brown silt with some gastropods and contains a layer of fire ash and charcoal that is continuous east of the graben. In the graben, u135 is best seen near meter 10 on the north wall

(Fig. 5). The contact between u135 and u130 is mostly obscured by bioturbation on the south wall. Unit u140 is a brown, organic-rich silt that overlies the blocky component of BSC2 and grades into its upper part. Unit u150 is a gray, sandy silt, underlying a markedly different unit, u200, a dark brown organic silty clay. Above u200 is a brown, sandy silt, unit u250, which overlies a blocky scarp colluvium, BSC3, near meter 6 (Figs. 4–7). Unit u300 is dark brown, organic silty clay. Unit u350 is brown sandy silt. Unit u400 is a thin (2–10 cm), dark brown, organic clayey silt. Unit u450 is brown sandy silt. Unit u500 is a brown to dark brown silt that has increasingly greater development of blocky peds eastward from the center of the graben. Recent artificial fills (containing asphalt and a bottle ca. 1960 at its base), unit u550, between 0.5 m and a few meters thick now cover most of the area west of the fault.

Appendix 2

Radiocarbon Ages on Humic Acids, Soil Fungus, and Shells

The dating of humic acids extracted from individual, detrital charcoal pieces has become feasible with the greatly reduced sample-size requirement of the AMS radiocarbon method. The effective standard pretreatment steps of charcoal consists of an acid wash to remove absorbed fulvic acids, followed by an alkali wash to remove absorbed humic acids. Both the fulvic and humic acids are generally considered possible contaminants of the charcoal and hence are routinely discarded. However, because we are not genuinely interested in the age of the charcoal, but rather the age of the layer, this approach may well be limited. As an exploratory test, we dated nine pairs of samples consisting of humic acid extracted from dated detrital charcoal pieces at the site. Seven pairs were from trench 00A (Table A1) and two from trench 00B (sample 00B1: humic age, 2350 ± 50 yr; charcoal age, 2250 ± 40 yr; sample 00B2: humic age, 1340 ± 50 yr; charcoal age, 1150 ± 50 yr). The results from all these samples indicate that, at 2σ , the humic acid ages range from the age of the charcoal to younger ages, but not younger than the overlying layers. Hence, the age of the humic acids appears to be linked to the age of deposition or burial of the sediment layer and/or the charcoal itself. Two issues require consideration when interpreting humic acid ages. First, what is the source of carbon? Secondly, how was the humic acid transported and sequestered? Humic acids form during the decomposition of organic matter, and hence we speculate that the humic acids extracted from charcoal consist of a mix derived from the decomposition of the charcoal and nearby organic matter. The ratio of mixing from these older and younger carbon sources gives rise to the variable age difference among sample pairs. The critical observation in our data is that the youngest humic acid ages from a layer are no younger than the overlying layers. We would expect a wider variation in ages, including older

Table A1
Radiocarbon Ages of Samples from Trench 00A

Sample No. (00A#)	¹⁴ C age (yr) BP, corrected*	Sample type [†]	Unit no. (u#)	Wall	Location (y. coord.) (m)	$\delta^{13}\text{C}^{\ddagger}$	CAMS no. [§]
1	550 ± 40	c	100	S	10–11	–25	68696
1h	680 ± 50	h	100	S	10–11	–28	69161
2	250 ± 40	fn	140	S	8.5–9	–25	68487
2a	350 ± 40	f	140	S	8.5–9	–25	69162
3	3670 ± 90	c	30	N	12–13.5	–25	68697
4	3640 ± 120	c	40	S	12.5–13.5	–25	68698
4h	2600 ± 110	h	40	S	12.5–13.5	–28	69163
4s	2840 ± 40	s	40	S	12.5–13.5	–5	68699
5	2760 ± 50	c	40	S	11–12	–25	68700
5h	1980 ± 40	h	40	S	11–12	–28	69235
6	610 ± 50	c	140	S	8.5–9	–25	69164
7	960 ± 40	c, ao	200	S	8.5–9	–25	69165
8	270 ± 50	c	350	S	8–9	–25	69166
9	210 ± 40	c, ao	450	S	8.5–9	–25	69167
10	1050 ± 50	c	200	S	7–8	–25	69168
11	400 ± 40	f	135	N	7–8.5	–25	69722
12	690 ± 40	f	200	N	10–11	–25	69723
14	210 ± 40	f	200	N	7–8.5	–25	69724
15	180 ± 40	c	350	N	7–8.5	–25	69904
15h	210 ± 60	h	350	N	7–8.5	–29	69726
17	1470 ± 40	c	100	N	8.5–10	–25	69905
18	1420 ± 70	c	200	N	6–7	–25	69789
18h	230 ± 40	h	200	N	6–7	–29	69727
19	2430 ± 40	s	135	N	7–8.5	–5	69906
20	990 ± 50	c	130	N	7–8.5	–25	69790
20h	680 ± 50	h	130	N	7–8.5	–29	69728
20s	2800 ± 40	s	130	N	7–8.5	–5	69907
21	1460 ± 60	c	200	S	6.5–7	–25	69791
21f	1720 ± 40	f	200	S	6.5–7	–25	69730
22	1140 ± 50	c	200	S	6.5–7	–25	69792
23	3840 ± 40	s	300	S	8–9	–5	69908
24	1330 ± 50	c	80	N	12–13.5	–25	69793
24h	1120 ± 40	h	80	N	12–13.5	–29	69729
26	2240 ± 50	s	40	S	13.5–14	–5	69909
27	2350 ± 50	s	40	S	13.5–14	–5	69910
30p	290 ± 50	p	135	N	9–11	–25	76313
30h	330 ± 40	h	135	N	9–11	–27.5	76169
31	850 ± 40	c	100	S	9.5–10	–26.9	72241
32	1090 ± 40	c	90	S	9.5–10	–27.9	72242
33	510 ± 50	c	100	S	9.5–10	–25.1	72243
39	1080 ± 50	c	80	S	6–6.5	–25.6	72244
40	310 ± 30	f	135	N	9–11	–23.4	76162
44	300 ± 110	c	135	N	9–11	–25	76314
53	1110 ± 40	c	80	S	12.5–13.5	–27.3	72245
60	2010 ± 30	c	135	N	9–11	–25	76315
60f	160 ± 50	f	135	N	9–11	–25	76316
60fh	350 ± 50	F, h	135	N	9–11	–27	76170
69	890 ± 40	c	110	S	8.5–9	–25.3	72246
71	730 ± 50	seeds	100	S	8–9	–27.9	72247
76	1350 ± 60	c	60	S	11–12	–26	72248
77	1140 ± 40	c	80	S	12.5–13.5	–25.9	72249

*Ages corrected for $\delta^{13}\text{C}$ (Stuiver and Pollach, 1977).

[†]c: charcoal acid–alkali-acid; c, ao: charcoal acid only; h: humic acids extracted from charcoal unless noted; f: soil fungus acid only; fn: soil fungus no pretreatment; p: plant fibers acid–alkali-acid; s: shell, splits indicated by matching sample numbers

[‡] $\delta^{13}\text{C}$ value without decimal are estimated with ± 2 (Stuiver and Pollach, 1977).

[§]All ages obtained by AMS analysis at the Center for Accelerator Mass Spectrometry (CAMS), Lawrence Livermore National Laboratory, Livermore, California.

humic-acid ages, if significant quantities of humic acids were being transported long distances (many meters laterally and vertically) from younger and older sediments in the section. Another observation that supports a lack of significant transport is that humic acids, sampled less than a meter from the present ground surface (sample 00A15, Fig. 5), do not show as a young an age as might be expected if the humic acids were derived from the modern soil. Because the site floods annually, saturated soil groundwater conditions should only facilitate humic-acid transport, and yet we see no evidence of this.

We caution that this application of humic acid dating is experimental and that individual site conditions require careful consideration. However, at this site, although we do not fully understand the processes of formation, migration, and absorption of humic acids, we infer that these ages seem to provide reliable estimates of depositional layer ages. This conclusion is based on the empirical evidence from this site alone.

The soil fungus consists of variable size aggregates up to 1 cm, of fungus spheres approximately 0.1 mm in size. Without microscopic identification, these samples are easily mistaken for weathered charcoal. They do not exhibit the more brilliant luster provided by the charcoal needles, but rather they appear dull. The source of carbon in soil fungus is not clear, as soil fungus often lives adjacent to or on roots. Thus, fungus may metabolize either older soil organic matter, including old charcoal, or modern carbon from roots, but most likely a combination. Due to this uncertainty, we decided not to use these results, even though the ages are reasonable and do not violate the age versus depth relationships of other types of samples that we consider reliable. This

result suggests that the soil fungus samples at our site formed not much later than layer deposition and did not acquire much carbon from younger intrusive roots.

Shells are constructed from carbon dissolved in water, which often is not in ^{14}C equilibrium with the atmosphere. The shell dating results from unit u40 and the overlying units u130/u135 range from 2200 to 2700 yr and 2300 yr to 2700 yr, respectively. The similarity of these ages suggests that either these shells formed at the same time and the overlying shells are reworked, or the levels of ^{14}C in the water were relatively constant in this age range. The distribution of these shell layers with respect to the graben makes reworking possible, although the high concentration of shells within layers would favor the second explanation. Due to these uncertainties, we did not use any shell ages in our event chronology.

U.S. Geological Survey 977
Menlo Park, California 94025
jlienk@usgs.gov
(J.L., T.D., D.S.)

U.S. Geological Survey
MS 966, Denver Federal Center
Denver, Colorado 80225
(S.P.)

Lawrence Livermore National Laboratory
Livermore, California 94551
(G.S.)

Department of Geography
University of California, Berkeley, California 94720
(L.R.)

Manuscript received 2 July 2001.